Lattice calculation of composite dark matter form factors

T. Appelquist, R. C. Brower, M. I. Buchoff, M. Cheng, S. D. Cohen, G. T. Fleming, J. Kiskis, M. F. Lin, E. T. Neil, J. C. Osborn, C. Rebbi, D. Schaich, C. Schroeder, S. Syritsyn, G. Voronov, P. Vranas, and J. Wasem (Lattice Strong Dynamics (LSD) Collaboration)

Phys. Rev. D **88**, 014502 — Published 2 July 2013

DOI: 10.1103/PhysRevD.88.014502

FERMILAB-PUB-13-014-T, LLNL-JRNL-608695, NT-LBL-13-002, UCB-NPAT-13-002

Lattice calculation of composite dark matter form factors

T. Appelquist,[1] R. C. Brower,[2] M. I. Buchoff,[3] M. Cheng,[4] S. D. Cohen,[4] G. T. Fleming,[1] J. Kiskis,[5] M. F. Lin,[1] E. T. Neil,[6] J. C. Osborn,[7] C. Rebbi,[2] D. Schaich,[8] C. Schroeder,[3] S. Syritsyn,[9] G. Voronov,[1] P. Vranas,[3] and J. Wasem[3]

(Lattice Strong Dynamics (LSD) Collaboration)

[1]*Department of Physics, Sloane Laboratory, Yale University, New Haven, Connecticut 06520, USA*
[2]*Department of Physics, Boston University, Boston, Massachusetts 02215, USA*
[3]*Lawrence Livermore National Laboratory, Livermore, California 94550, USA*
[4]*Department of Physics, University of Washington, Box 351560, Seattle, WA 98195, USA*
[5]*Department of Physics, University of California, Davis, California 95616, USA*
[6]*Theoretical Physics Department, Fermi National Accelerator Laboratory, Batavia, IL 60510, USA*
[7]*Argonne Leadership Computing Facility, Argonne, Illinois 60439, USA*
[8]*Department of Physics, University of Colorado, Boulder, CO 80309, USA*
[9]*Lawrence Berkeley National Laboratory, Berkeley, CA 94720, USA*

Composite dark matter candidates, which can arise from new strongly-coupled sectors, are well-motivated and phenomenologically interesting, particularly in the context of asymmetric generation of the relic density. In this work, we employ lattice calculations to study the electromagnetic form factors of electroweak-neutral dark-matter baryons for a three-color, QCD-like theory with $N_f = 2$ and 6 degenerate fermions in the fundamental representation. We calculate the (connected) charge radius and anomalous magnetic moment, both of which can play a significant role for direct detection of composite dark matter. We find minimal N_f dependence in these quantities. We generate mass-dependent cross-sections for dark matter-nucleon interactions and use them in conjunction with experimental results from XENON100, excluding dark matter candidates of this type with masses below 10 TeV.

PACS numbers: 11.10.Hi, 11.15.Ha, 95.35.+d

Introduction Experimental bounds on the interaction of the dark matter with Standard-Model (SM) particles have strengthened by many orders of magnitude in recent years. In particular, dark-matter particles cannot have SM-strength couplings to electroweak gauge bosons, based on direct-detection constraints [1, 2]. At the same time, there is a strong motivation for the dark matter to couple to the SM in some way for the purpose of relic density generation, either as a thermal relic via the so-called "WIMP miracle" (see [3] for a recent review) or through an asymmetric scenario which may be related to the creation of baryon asymmetry [4–11]. Construction of dark matter models thus requires a careful balance between the presence and absence of dark-sector interactions with the SM.

Composite dark matter models provide a simple mechanism for attaining this balance, one which can lead to interesting and unique phenomenology. By hypothesizing a new, confining gauge force in the dark sector, an electroweak-neutral composite dark matter candidate can be constructed as a bound state of electroweak-charged constituents. In this way, electroweak interactions can be active in the early Universe for the generation of relic density, but only neutral bound states survive to the present day. Electroweak coupling to the constituents is still possible, leading to form-factor suppressed interactions with the neutral composites. They can be roughly estimated from QCD analogs, but in general can be determined quantitatively only by lattice calculations.

In this paper, we consider an underlying $SU(3)$ gauge theory with fermions in the fundamental representation, but focus on fermions not associated with electroweak breaking. We use $SU(3)$ because much is known about it from lattice QCD and because we have already generated lattice vacuum states of $SU(3)$ with 2 and 6 fundamental flavors on large lattices [12, 13]. We take the fermions to be mass-degenerate $SU(2)_L$ singlets such that $Q = Y$. We consider a two-fermion theory ($N_f = 2$) with $Q_u = 2/3$ and $Q_d = -1/3$, as well as a six-fermion theory ($N_f = 6$) with three such pairs of fermions. In either case, the lightest baryon is expected to be electrically neutral, and will therefore also have vanishing weak charge. The dominant contribution to its interaction with ordinary nuclei will be due to single photon exchange, which can be parameterized primarily in terms of its magnetic moment and charge radius. In these initial lattice calculations we consider only quark-line connected contributions to the charge radius and magnetic moment. We compute the electromagnetic form factors of this particle to extract these quantities, describe their dependence on N_f, and discuss consequences for direct detection.

One could also modify or enlarge the fermion content of the $SU(3)$ gauge theory to include $SU(2)_L$-doublet fermions. This would be a necessary modification in order to consider composite dark matter arising in a theory of dynamical electroweak symmetry breaking [4–9, 14–20]. Careful model building is then required to ensure that the lightest baryon is net electroweak neutral. We do not discuss this possibility here.

Model setup For the theory with $SU(2)_L$-singlet fermions carrying charges $Q_u = 2/3$ and $Q_d = -1/3$, with $N_f = 2$ or 6, the analogue of the neutron ($N \sim udd$) will be the dark matter candidate, with mass M_B and carrying no net electroweak charge. It is stabilized by conservation of dark baryon number. The other charged baryons are expected to be heavier due to electromagnetic mass corrections of order $\Delta M \sim \alpha M_B/4\pi$. We include a fermion mass m_f, essential for lattice calculation purposes, and examine dependence on m_f for a range $m_f \ll M_B$.

Our dark sector also contains $N_f^2 - 1$ pseudo-Nambu-Goldstone-boson (PNGB) states. We assume that these states are unstable, decaying to Standard-Model particles with a sufficient rate that their presence does not influence the cosmological history of the Universe.

As our focus is on direct-detection signatures, we do not consider the dark matter generation in detail here. The confinement scale Λ, or equivalently the dark matter mass M_B, is a free parameter in our construction.

Electromagnetic Form Factors Since the neutral baryon in the $SU(2)$-singlet theory is the dark matter candidate of interest [39], the baryon mass M_B (degenerate in the absence of other interactions) is the dark matter mass. This mass and all other dimensionful quantities are expressed in lattice units here.

The quantities of central interest here are the Dirac and the Pauli electromagnetic form factors of a neutral dark-matter baryon $|N(p)\rangle$. For the $N_f = 2$ case, they can be expressed in terms of matrix elements of the vector currents of individual quarks as follows:

$$\begin{aligned}&\langle N(p')|\overline{\psi}\gamma^\mu\psi|N(p)\rangle\\&\quad= \overline{U}(p')\left[F_1^\psi(Q^2)\gamma^\mu + F_2^\psi(Q^2)\frac{i\sigma^{\mu\nu}q_\nu}{2M_B}\right]U(p)\,,\end{aligned} \tag{1}$$

where $\psi = u, d$ are quark fields, U, $\overline{U}$ are on-shell baryon spinors, $q = p' - p$, and $Q^2 = -q^2 > 0$ is the momentum transfer. In the forward limit $Q^2 = 0$, the Dirac form factors are equal to the numbers of the valence quarks: $F_1^u(0) = 1$ and $F_1^d(0) = 2$.

From these one constructs the isovector and isoscalar form factors[40]:

$$\begin{aligned}F_{1,2}^v(Q^2) &= F_{1,2}^d(Q^2) - F_{1,2}^u(Q^2)\,,\\F_{1,2}^s(Q^2) &= F_{1,2}^d(Q^2) + F_{1,2}^u(Q^2)\,.\end{aligned} \tag{2}$$

Both of these quantities can be extracted from lattice calculations, but the isoscalar contribution contains expensive disconnected lattice quark contractions, which cancel in the isovector case, and as a result, isovector form factors are far more tractable. While we ultimately will calculate the disconnected pieces of the isoscalar form factor as well, this work will focus on only the connected contributions.

For the $N_f = 6$ case, with three pairs of $u(Q = 2/3)$ and $d(Q = -1/3)$ fermions, we take the $|N(p)\rangle$ state to be composed of fermions from only one pair. Since we omit disconnected lattice quark contractions in our calculation, it is only the currents $\overline{\psi}\gamma^\mu\psi$ composed of the fermion fields from the same pair that contribute to the computed electromagnetic form factors. Therefore, in our calculation the other two pairs play a role in only the strong dynamics of the $SU(3)$ gauge theory.

The full electromagnetic form factors of the neutral dark baryon[41] are given by

$$\begin{aligned}F_{1,2;\text{neut}}(Q^2) &= Q_u F_{1,2}^u(Q^2) + Q_d F_{1,2}^d(Q^2)\\&= \frac{1}{6}F_{1,2}^s(Q^2) - \frac{1}{2}F_{1,2}^v(Q^2)\,;\end{aligned} \tag{3}$$

since $F_1^s(0) = 3$ and $F_1^v(0) = 1$, the total charge $F_{1;\text{neut}}(0) = 0$. For soft single-photon exchange scattering, only the forward ($Q^2 \to 0$) behavior of the electromagnetic form factors is relevant. Since the electric charge $F_{1;\text{neut}}(0)$ is zero, only the magnetic moment $\mu_{\text{neut}} = \kappa_{\text{neut}}$ and the Dirac radius $\langle r^2_{1;\text{neut}}\rangle$ contribute to the scattering amplitude to the lowest order in Q^2:

$$\begin{aligned}F_{1;\text{neut}}(Q^2) &= -\frac{1}{6}Q^2\langle r^2_{1;\text{neut}}\rangle + \mathcal{O}(Q^4)\,,\\F_{2;\text{neut}}(Q^2) &= \kappa_{\text{neut}} + \mathcal{O}(Q^2)\,,\end{aligned} \tag{4}$$

The Dirac charge radius $\langle r^2_{1;\text{neut}}\rangle$ determines the slope of the form factor in the $Q^2 \to 0$ limit:

$$\langle r^2_{1;\text{neut}}\rangle \overset{def}{=} -6\frac{dF_{1;\text{neut}}(Q^2)}{dQ^2}\Big|_{Q^2=0}\,. \tag{5}$$

The definition of the radius (5) is motivated by the algebraic identity

$$\int d^3r\, r^2\,\rho(r) \equiv -6\frac{dF_1(Q^2)}{dQ^2}\Big|_{Q^2=0}\,, \tag{6}$$

where $\rho(r)$ is the "charge density",

$$\int d^3r\, e^{i\vec{q}\vec{r}}\,\rho(r) = F_1(Q^2)\,,\quad Q^2 \underset{non-rel.}{\approx} \vec{q}^{\,2}\,, \tag{7}$$

which has physical meaning if and only if the spatial extent of this distribution is much larger than the Compton wave length of the composite particle, $\langle r^2\rangle \gg M_B^{-2}$. Since the total charge, $\int d^3r\,\rho(r) \equiv F_1(0)$, is zero, the charge density must have alternating sign (or be exactly zero), and the integral in Eq. (6) can be either positive or negative.

For the following, we also need to define the *mean squared charge radius* $\langle r_E^2\rangle$, or the "radius" of the charge form factor $G_E(Q^2)$,

$$G_E(Q^2) = F_1(Q^2) - \frac{Q^2}{4M_B^2}F_2(Q^2)\,. \tag{8}$$

Similar to Eq. (5), the charge radius of the neutral baryon is equal to

$$\langle r^2_{E;\text{neut}}\rangle \overset{def}{=} -6\frac{dG_{E;\text{neut}}(Q^2)}{dQ^2}\Big|_{Q^2=0} = \langle r^2_{1;\text{neut}}\rangle + \frac{3\kappa_{\text{neut}}}{2M_B^2}\,, \tag{9}$$

differing from the Dirac radius by only the relativistic correction $\sim M_B^{-2}$ (the Foldy term). This correction is important if the size of the particle is comparable to its Compton wave length, which is the case for the neutron and the proton in QCD.

The (anomalous) magnetic moment of the neutral baryon is related to the isovector and isoscalar moments as

$$\kappa_{\text{neut}} = \frac{1}{6}\kappa_s - \frac{1}{2}\kappa_v\,. \tag{10}$$

The isovector and isoscalar Dirac form factors are not zero in the forward limit. Their radii are defined to be independent of their overall normalization,

$$F_1^{v,s}(Q^2) = F_1^{v,s}(0)\big[1 - \frac{1}{6}Q^2\langle r_1^2\rangle^{v,s} + O(Q^4)\big]\,. \tag{11}$$

The radii of the neutral baryon are related to the isovector and isoscalar radii as follows:

$$\begin{aligned}\langle r^2_{1;\text{neut}}\rangle &= \frac{1}{2}\langle r_1^2\rangle^s - \frac{1}{2}\langle r_1^2\rangle^v\,,\\ \langle r^2_{E;\text{neut}}\rangle &= \frac{1}{2}\langle r_E^2\rangle^s - \frac{1}{2}\langle r_E^2\rangle^v\,.\end{aligned} \tag{12}$$

Simulation Details Lattice calculations are performed using $32^3 \times 64$ domain-wall lattices with the Iwasaki improved gauge action and a fifth-dimensional length $L_s = 16$ and a domain-wall height of $m_0 = 1.8$. By using domain-wall fermions, the calculation preserves exact flavor symmetry, and chiral-breaking lattice spacing artifacts are suppressed. The calculation is performed for $N_f = 2$ at $\beta = 2.70$ and $N_f = 6$ at $\beta = 2.10$. The beta values are tuned to match the confinement scale of both theories relative to the lattice spacing, including M_B as we shall see below. For both $N_f = 2$ and $N_f = 6$, five separate mass points are analyzed with $m_f = 0.010, 0.015, 0.020, 0.025, 0.030$. The pion masses (in units of the nucleon mass) are $0.41 \le m_\pi/M_B \le 0.52$ and $0.44 \le m_\pi/M_B \le 0.52$ for $N_f = 2$ and $N_f = 6$, respectively. Further details and other results from these ensembles are given in [12, 13, 21].

Calculation and Fitting The parameters of interest are extracted from two sets of correlation functions: two-point correlation functions given by

$$C_{NN}(\tau,\mathbf{p}) = \sum_{\mathbf{x}} e^{-i\mathbf{p}\cdot\mathbf{x}}\langle N(\mathbf{x},\tau)\bar{N}(0)\rangle, \tag{13}$$

and three-point correlation functions

$$\begin{aligned}C_{N\mathcal{O}N}(\tau,T,\mathbf{p},\mathbf{p}') = &\sum_{\mathbf{x},\mathbf{y}} e^{-i\mathbf{p}'\cdot\mathbf{x}+i(\mathbf{p}'-\mathbf{p})\cdot\mathbf{y}}\times\\ &\times\langle N(\mathbf{x},T)\mathcal{O}(\mathbf{y},\tau)\bar{N}(0)\rangle\,,\end{aligned} \tag{14}$$

where $\mathcal{O}(\mathbf{y},\tau)$ is the quark vector current density operator.

The long-distance limit of the Euclidean time behavior of these correlation functions is given by

$$C_{NN}(\tau,\mathbf{p}) \overset{\tau\gg\frac{1}{\Delta}}{\longrightarrow} \frac{Z(\mathbf{p})e^{-E\tau}}{2E}\mathrm{Tr}\Big[\Gamma_{\text{pol}}(i\not{p} + M_B)\Big]\,, \tag{15}$$

$$\begin{aligned}C_{N\mathcal{O}N}(\tau,T,\mathbf{p},\mathbf{p}') &\overset{T,\tau\gg\frac{1}{\Delta}}{\longrightarrow} \frac{\sqrt{Z(\mathbf{p})Z(\mathbf{p}')}e^{-E'(T-\tau)-E\tau}}{4EE'}\times\\ &\times\mathrm{Tr}\Big[\Gamma_{\text{pol}}(i\not{p}' + M_B)\Gamma^\mu(i\not{p} + M_B)\Big]\,,\end{aligned} \tag{16}$$

where Γ_{pol} is the polarization matrix of the initial and final baryon spin states corresponding to Eq. (13,14), Γ^μ is the fermion vertex function (cf. Eq.(1)),

$$\Gamma^\mu = F_1(Q^2)\gamma^\mu + F_2(Q^2)\frac{\sigma^{\mu\nu}q_\nu}{2M_B}\,, \tag{17}$$

and Δ is the difference in energy between the ground and the first excited state of the baryon. More details on the form factor calculation on the lattice can be found in Ref. [22].

We use the standard widely adopted "ratio" method in order to extract hadron matrix elements from corresponding two- and three-point functions,

$$\begin{aligned}R_{\mathcal{O}}(\tau,T,\mathbf{p},\mathbf{p}') = &\frac{C_{N\mathcal{O}N}(\tau,T,\mathbf{p},\mathbf{p}')}{\sqrt{C_{NN}(T,\mathbf{p})C_{NN}(T,\mathbf{p}')}}\times\\ &\times\sqrt{\frac{C_{NN}(T-\tau,\mathbf{p})C_{NN}(\tau,\mathbf{p}')}{C_{NN}(T-\tau,\mathbf{p}')C_{NN}(\tau,\mathbf{p})}},\end{aligned} \tag{18}$$

where the long Euclidean time behavior yields

$$\begin{aligned}R_{\mathcal{O}}(\tau,T,\mathbf{p},\mathbf{p}') &\overset{T,\tau\gg\frac{1}{\Delta}}{\longrightarrow} \langle N(\mathbf{p}')|\mathcal{O}|N(\mathbf{p})\rangle\\ &+\mathcal{O}(e^{-\Delta\tau}) + \mathcal{O}(e^{-\Delta(T-\tau)}) + \mathcal{O}(e^{-\Delta T})\end{aligned} \tag{19}$$

We analyze these ratios for multiple initial and final momentum combinations and vector current components in order to extract form factors F_1 and F_2. Their values form a reasonable "plateau" as functions of τ, the timeslice of the current operator insertion, indicating absence of significant excited-state contaminations (see Fig. 1).

In general, excited states can cause significant systematic errors in three-point functions and hadron matrix elements [23]. We compute our form factor values as averages of three central points in the plateaus.

The form factors $F_{1,2}(Q^2)$ are calculated at discrete values of the momentum transfer $Q^2 \approx (\mathbf{p}' - \mathbf{p})^2$ determined by the lattice volume. We interpolate the Dirac and isovector Pauli form factors using a dipole formula fit

$$F_{1,2}(Q^2) \sim \frac{A_{1,2}}{(1 + B_{1,2}Q^2)^2} \tag{20}$$

motivated by nucleon form factor phenomenology. The isoscalar Pauli form factor turns out to be very close to zero, and the dipole form that has definite sign does not necessarily yield a stable fit to the data; therefore, we use the linear fit $F_i(Q^2) \sim F_i(0) + F_i'(0)Q^2$. Examples of fits are shown on Fig. 2. We use these fits to interpolate (extrapolate in the case of Pauli form factors) near the forward limit $Q^2 = 0$ in order to determine κ and $\langle r_1^2\rangle$.

Lattice Results

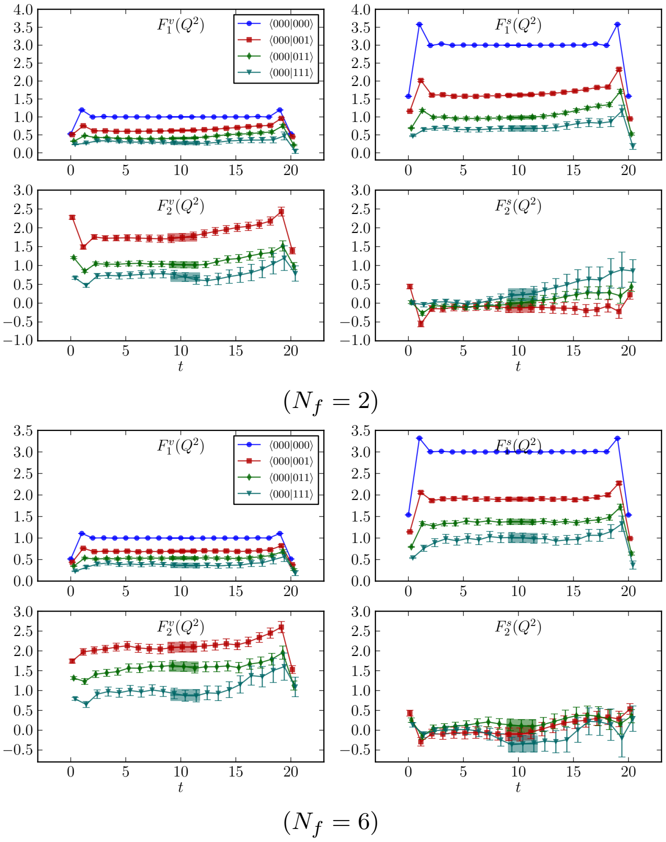

FIG. 1: (color online) Examples of form factor plateaus for $m_f = 0.015$ for 2 and 6 flavors. Form factor plateaus are shown for all values of Q^2 for F_1 and for $Q^2 > 0$ for F_2; corresponding lattice initial and final momenta are shown in the legends.

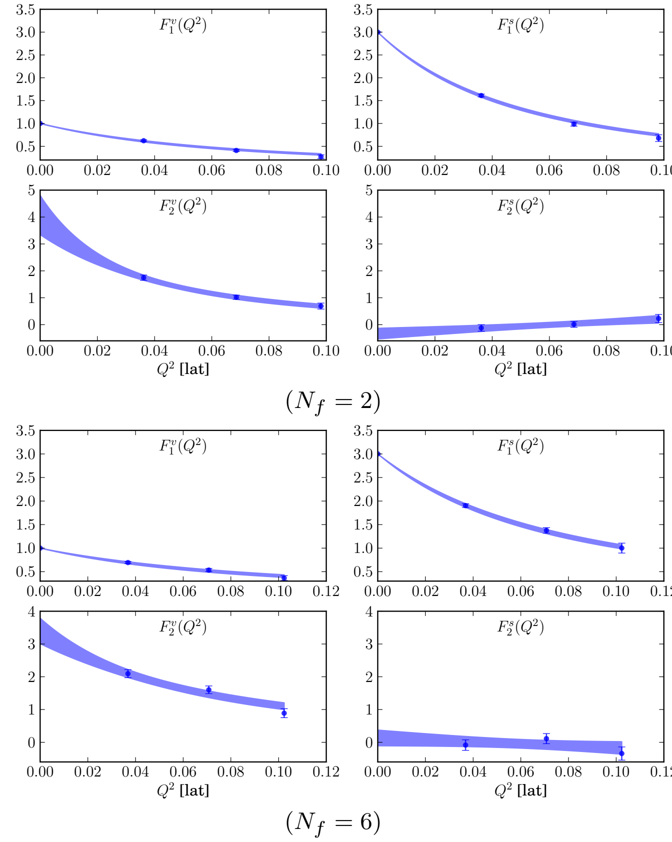

FIG. 2: Examples of Q^2 fits of Dirac and Pauli form factors $F_{1,2}(Q^2)$ for $m_f = 0.015$ for 2 and 6 flavors. The bands show the dipole fits for all form factors except F_2^s, for which we used the linear fit for $Q^2 \to 0$ extrapolation.

Baryon Mass The dark-matter baryon mass is plotted as a function of the fermion mass m_f in Fig. 3. A linear dependence of the baryon mass on m_f can be seen for both theories, as expected in the calculation regime where the fermion masses are small. In the absence of additional interactions, a finite value of m_f is required to give mass to the PNGB's of the theory, but we nevertheless perform a linear fit in order to extract the chiral-limit baryon mass M_{B_0}. This scale, which can be taken as a proxy for the confinement scale of the theory, serves as a common reference scale for the calculation results with $m_f \geq 0$.

Anomalous magnetic moment The anomalous magnetic moment is the most important for direct detection experiments. It enters at the dimension-5 level in the baryon effective field theory and arises as the zero-momentum value of the Pauli form factor, $F_2(0)$. The isovector Pauli form factor, giving κ_v, is under most control since all expensive disconnected contributions cancel due to isospin symmetry. The isoscalar channel, which is also necessary to determine κ_{neut}, has both connected and disconnected contributions to the three-point correlation function. In this initial work, we omit the disconnected contributions and assume the connected pieces dominate the isoscalar contribution.

We plot the anomalous magnetic moment κ_{neut}, computed as described above, versus M_B/M_{B_0} in Fig. 4. It shows little dependence on the mass and little dependence on the number of fermions. The $N_f = 2$ results $\kappa_{\text{neut}} \approx -(1.71 \ldots 2.09)$ are consistent with the measured neutron value $\kappa = -1.91$ [24]. Calculations of nucleon structure with $N_f = 2$ Wilson fermions were previously reported in Ref.[25], which found values $\kappa_{\text{neut}} \approx -(1.30 \ldots 1.45)$, with the difference coming predominantly from the isovector Pauli form factor; our results for this form factor more closely match the more recent results of [26, 27].

Charge radius While the charge radius is expected to lead to a smaller effect on the spin-independent cross section as compared to the magnetic moment, it could have a significant effect if its value depends significantly on N_f. It is therefore informative to explore the relative size of the charge radius contribution to the spin-independent cross section. As with the magnetic moment, only the isovector charge radius is absent of disconnected lattice quark contractions, but we omit them for the isoscalar channel as well.

The results for the mean square charge radius $\langle r^2_{E;\text{neut}} \rangle$

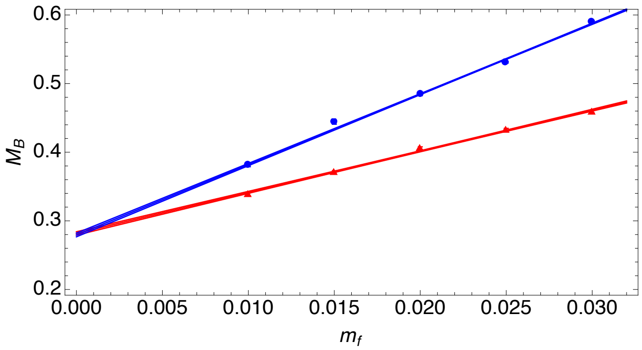

FIG. 3: Dark-matter baryon mass (in lattice units) with $N_f = 2$ (red) and $N_f = 6$ (blue), as a function of the fermion mass m_f (also in lattice units). The two data sets are extrapolated to obtain the chiral-limit baryon mass M_{B_0}, which is used to set a physical scale independent of am_f. With the chosen lattice couplings, M_{B_0} is the same within statistical precision in the $N_f = 2$ and $N_f = 6$ theories.

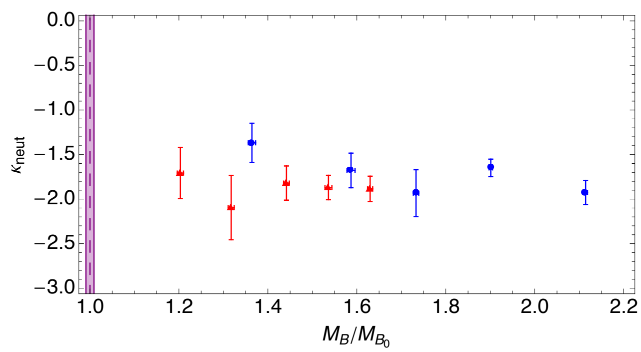

FIG. 4: The neutral baryon anomalous magnetic moment for $N_f = 2$ (red) and $N_f = 6$ (blue) theories versus dark-baryon mass. This quantity shows no systematic separation between two and six flavor theories.

of an electroweak-neutral dark-matter baryon are presented in Fig. 5. Note that the results are negative (see discussion after Eq. (6)). As in the case of the anomalous moment, our results show little dependence on N_f and little dependence on the dark-baryon mass as it varies due to changes in the underlying fermion mass. If the fermion mass is reduced further, bringing M_B/M_{B_0} closer to unity, the magnitude $\langle r^2_{E;\mathrm{neut}}\rangle$ is expected to grow. This is because the PNGB mass drops, and the charge radius is quite sensitive to the size of the PNGB cloud.

For $N_f = 2$, this point can be made more precisely by comparison to QCD. There, the mean squared charge radius of the neutron is also negative, $\langle r^2_{En}\rangle = -0.1161(22)\ \mathrm{fm}^2$ [24]. Our $N_f = 2$ calculation corresponds to QCD with $M_B \approx 1$ GeV, but with relatively heavy underlying quarks, and thus relatively heavy pions: the pion mass in units of M_B ranges between the lightest $m_\pi/m_B = 0.41$ to the heaviest $m_\pi/m_B = 0.52$. In QCD units, our lattice spacing is given by $a \approx 0.055$ fm,

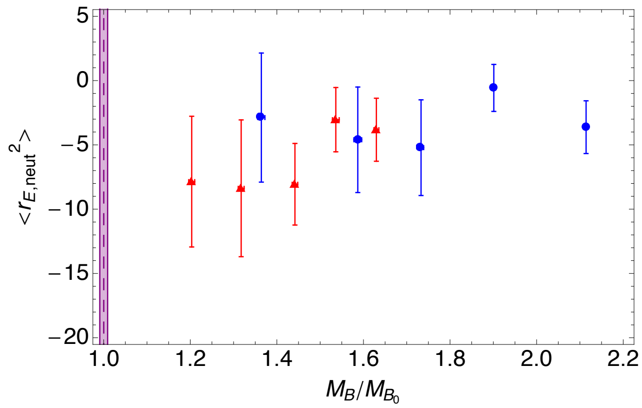

FIG. 5: The neutral baryon mean squared charge radius (in lattice units) for $N_f = 2$ (red) and 6 (blue), versus dark-baryon mass. Again, no significant systematic difference between the two theories is seen over the range of masses considered.

so our result is $\langle r^2_{E,neut}\rangle \approx -(0.009\ldots0.025)\ \mathrm{fm}^2$, substantially less than the observed result. Previous calculations of nucleon structure with $N_f = 2$ Wilson fermions [25] yielded similar values $\langle r^2_{E,\mathrm{neut}}\rangle = -(0.011\ldots0.023)\ \mathrm{fm}^2$. These results, too, employed relatively heavy underlying quarks. In our case, further studies with smaller fermion mass can shed light on the range of direct detection allowed values for the mean square charge radius.

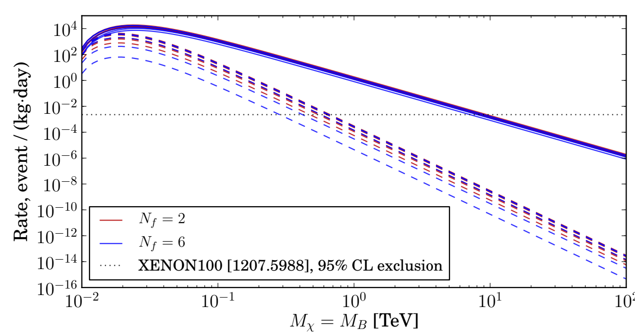

FIG. 6: Calculated XENON100 event rates based on energy cuts and acceptance rates from Ref. [28] (solid lines). For comparison, we also show scattering rates using only the charge radius term, which is suppressed by two additional powers of M_χ (dashed lines). The experimental upper bound on event rates, based on accumulated 2323.7 kg·days of exposure [28] are shown with the dotted lines.

Direct detection exclusion plots We next compare our calculations of dark-matter parameters with the current experimental bounds on the dark-matter-nucleus cross-sections in direct detection experiments. Currently, the most stringent bound is provided by the XENON100 experiment [28], in which hypothetical dark-matter particles are detected through their collisions with xenon nuclei with $Z = 54$ and $A = 124\ldots136$, and which has accumulated

2323.7 kg·days of effective exposure. Two of the isotopes, ^{129}Xe and ^{131}Xe, have non-zero spin and are sensitive to the spin-dependent $M1$ interaction. Their combined abundance constitutes approximately 1/2 in natural xenon [29].

In this section, we adopt a more conventional notation M_χ for the mass of the dark-matter particle, and also denote its radius and magnetic moment with a subscript "χ". Figs. 4 and 5 show that the anomalous moment and mean square charge radius vary little with the amount of the dark-matter mass coming from the underlying fermion mass (and also vary little as N_f is increased from 2 to 6).

The differential cross-section of a dark-matter fermion and a nucleus, to leading order in the non-relativistic dark-matter velocity $v \ll 1$ is

$$\frac{d\sigma}{dE_R} = \frac{\overline{|\mathcal{M}_{\text{SI}}|^2} + \overline{|\mathcal{M}_{\text{SD}}|^2}}{16\pi(M_\chi + M_T)^2 E_R^{\max}}\,, \tag{21}$$

where M_T is the mass of the target nucleus, and $E_R^{\max} = \frac{2M_\chi^2 M_T v^2}{(M_\chi+M_T)^2}$ is the maximal recoil energy for given collision velocity v. The quantities and $\overline{|\mathcal{M}_{\text{SI,SD}}|}^2$ are spin-(in)dependent amplitudes squared, averaged over initial and summed over final states:

$$\begin{aligned}\overline{|\mathcal{M}_{\text{SI}}|^2} = e^4 \left[Z F_c(Q)\right]^2 \left(\frac{M_T}{M_\chi}\right)^2 \Big[\frac{4}{9} M_\chi^4 \langle r_{E\chi}^2\rangle^2 \\ + \left(1+\frac{M_\chi}{M_T}\right)^2 \kappa_\chi^2 \cot^2\frac{\theta_{\text{CM}}}{2}\Big]\,,\end{aligned} \tag{22}$$

$$\overline{|\mathcal{M}_{\text{SD}}|^2} = e^4\,\frac{2}{3}\Big(\frac{J+1}{J}\Big)\left[\Big(A\frac{\mu_T}{\mu_n}\Big)\,F_s(Q)\right]^2 \kappa_\chi^2\,. \tag{23}$$

Here, Z and A are the charge and atomic numbers of a specific xenon isotope, (μ_T/μ_n) is the nucleus magnetic moment expressed in Bohr magnetons $\mu_n = \frac{e}{2m_n}$, $F_{c,s}(Q)$ are its nuclear charge and spin form factors, respectively, at the momentum transfer $Q \approx \sqrt{Q^2} = \sqrt{2M_T E_R}$, and θ_{CM} is the scattering angle in the center-of-mass frame [42]. For non-relativistic velocities, $\cot^2\frac{\theta_{\text{CM}}}{2} = \left(\frac{E_R^{\max}}{E_R} - 1\right)$.

For the nuclear response form factors $F_{c,s}(Q^2)$, we use the following commonly accepted phenomenological expressions [18, 30]:

$$|F_c(Q)|^2 = 9\left|\frac{\sin(QR_c) - (QR_c)\cos(QR_c)}{(QR_c)^3}\right|^2 e^{-(QS)^2}\,, \tag{24}$$

$$|F_s(Q)|^2 = \begin{cases} 0.047\,, & 2.55 \le QR_s \le 4.5\,,\\ \left|\frac{\sin(QR_s)}{QR_s}\right|^2\,, & \text{otherwise}\,,\end{cases} \tag{25}$$

where $R_c = 1.14 A^{1/3}$ fm, $R_s = 1.00 A^{1/3}$ fm, and $S = 0.9$ fm. The nuclear response functions $F_{c,s}(Q^2)$ can also be evaluated using nuclear models, as was done in Ref. [31, 32].

Following Refs. [18, 28], we compute the scattering rate for a range of dark-matter particle masses with the recoil energies $E_R = 6.6 \ldots 43.3$ keV:

$$R = \frac{M_{\text{detector}}}{M_T}\frac{\rho_{\text{DM}}}{M_\chi}\int_{E_{\min}}^{E_{\max}} dE_R\, \mathcal{A}cc(E_R)\left\langle v'\,\frac{d\sigma}{dE_R}\right\rangle_f\,, \tag{26}$$

where $\langle\cdot\rangle_f$ denotes averaging over the DM velocity distribution (27), $v' = |\vec{v} - \vec{v}_{\text{Earth}}|$ is the dark-matter velocity with respect to the detector (the Earth), and $\mathcal{A}cc(E_R)$ is the recoil energy-dependent acceptance rate of the detector [28]. We assume the thermal distribution of velocities in the galactic dark-matter halo [30],

$$\frac{d^3 n}{d\vec{v}^3} = f(\vec{v}) = \frac{1}{\pi^{3/2} v_0^3} e^{-\vec{v}^2/v_0^2}\,, \quad \int_{|\vec{v}|<v_{\text{esc}}} d^3\vec{v}\; f(\vec{v}) \equiv 1\,, \tag{27}$$

with $v_0 = v_{\text{Earth}} = 220$ km/s, $v_{\text{esc}} = 544$ km/s, and the dark-matter mass density $\rho_{\text{DM}} = 0.3\,\text{GeV/cm}^3$. Finally, we average the expected scattering rate over the natural xenon isotopic abundances.

We show computed scattering rates in Fig. 6 with solid lines. The accumulated XENON100 statistics [28] exclude composite dark matter particles with $M_\chi \lesssim 10$ TeV. With fixed values of the dimensionless quantities $M_\chi^2\langle r^2\rangle$ and κ computed on a lattice, the differential cross-section scales as

$$\frac{d\sigma}{dE_R} \sim \mathcal{A}\frac{(M_\chi^2\langle r_{E\chi}^2\rangle)^2}{M_\chi^4} + \mathcal{B}\frac{\kappa_\chi^2}{M_\chi^2}\,. \tag{28}$$

The charge radius contribution is suppressed as M_χ^{-2} relative to the magnetic moment contribution and becomes negligible with growing M_χ. In the scattering rate shown in Fig. 6, both contributions are additionally suppressed by the DM particle number density ρ_{DM}/M_χ as $M_\chi \to \infty$ (see Eq.(26)). The large-M_χ scaling of the charge radius term is shown in Fig. 6 with the dashed lines; it is evident that the total scattering rate (solid lines) is dominated by the magnetic moment term for dark matter masses $M_\chi \gtrsim 25$ GeV. Even if one were to make the charge radius as much as an order of magnitude larger by reducing the PNGB mass (see the discussion following Fig. 5), its contribution would still be negligible at $M_B = 10$ TeV, the lower limit of the allowed region.

Discussion We have studied the electromagnetic form factors of electroweak-neutral dark-matter baryons in an $SU(3)$ gauge theory with $N_f = 2$ and 6 $SU(2)_L$-singlet fermions, with charge assignments $+2/3$ and $-1/3$ (one pair or three pairs). These baryons have the desired properties of dark matter since they are stable, electroweak neutral, and can explain the relic density through the same early universe sphaleron process that describes baryogenesis.

Of particular interest to direct detection experiments are the anomalous magnetic moment and mean square charge radius of the dark-matter baryon. These parameters determine the observed cross-section with nuclei (in this work, we primarily focus on Xenon) due to (dominant) single-photon exchange. The contribution from the dark-matter anomalous moment dominates the charge-radius contribution for $M_\chi \gtrsim 25$GeV. However, in our calculation the charge radius $\langle r_E^2 \rangle$ turns out to be particularly small, much smaller than it is in QCD. Exploring smaller quark mass regions may change this balance and make the charge radius more relevant for the direct detection of the dark matter.

Examining the dark matter exclusion plots in light of the latest Xenon100 results [28], we conclude that in these theories, dark-matter masses less than 10 TeV are excluded. We have so far seen little dependence on N_f. It will be interesting to see whether this begins to change, even continuing to neglect disconnected quark contractions, as N_f is increased toward the edge of the conformal window ($N_f \approx 10 - 12$ for an $SU(3)$ gauge theory with fermions in the fundamental representation). When the disconnected contractions are included, additional N_f dependence will arise simply from the counting of these loop contributions.

As we have shown in this work, with non-zero magnetic moment the experimental constraints on the dark matter mass are quite stringent. This naturally motivates the consideration of even N_c theories, in which the baryons are bosonic and thus have no magnetic moment. Interactions can be further suppressed if the charge assignments are symmetric in such a way that the charge radius vanishes (see e.g. [19]), making the electromagnetic polarizabilities the dominant interactions. Some initial lattice work on the zero-temperature dynamics of such theories has been carried out in [33, 34], and we are currently planning similar calculations with an eye towards dark matter form factors.

Acknowledgements We thank the LLNL Multiprogrammatic and Institutional Computing program for Grand Challenge allocations and time on the LLNL BlueGene/L (uBGL) supercomputer as well as on the LLNL Hera, Atlas, and Zeus computing clusters. We thank LLNL for funding from LDRD 10-ERD-033 and LDRD 13-ERD-023. The LSD collaboration would like to thank Graham Kribs for his valuable input on this effort and for providing insightful comments on the manuscript draft. MIB would like to thank Graham Kribs for many illuminating and insightful discussion throughout this work, along with the hospitality of the University of Oregon particle theory group. SNS would like to thank Wick Haxton for helpful discussions on nuclear response form factors. Several of the authors would also like to thank the Kavli Institute for Theoretical Physics and the organizers of the program "Novel Numerical Methods for Strongly Coupled Quantum Field Theory and Quantum Gravity", where much of this work was developed. This work has been supported by the U. S. Department of Energy under Grant Nos. DE-FG02-04ER41290 (D.S.), DE-FG02-91ER40676 (R.C.B., M.C., C.R.), DE-FG02-92ER-40704 (T.A.) and Contracts DE-AC52-07NA27344 (LLNL), DE-AC02-06CH11357 (Argonne Leadership Computing Facility), and DE-AC02-07CH11359 (Fermi Research Alliance, LLC), and by the National Science Foundation under Grant Nos. NSF PHY11-00905 (G.F., M.L., G.V.) and PHY11-25915 (Kavli Institute for Theoretical Physics). S.N.S was supported by the Office of Nuclear Physics in the US Department of Energy's Office of Science under Contract DE-AC02-05CH11231.

[1] M. W. Goodman and E. Witten, Phys.Rev. **D31**, 3059 (1985).
[2] A. Kurylov and M. Kamionkowski, Phys.Rev. **D69**, 063503 (2004), hep-ph/0307185.
[3] D. Hooper, pp. 709–764 (2009), 0901.4090.
[4] S. Nussinov, Phys. Lett. **B165**, 55 (1985).
[5] S. M. Barr, R. S. Chivukula, and E. Farhi, Phys. Lett. **B241**, 387 (1990).
[6] D. B. Kaplan, Phys.Rev.Lett. **68**, 741 (1992).
[7] S. B. Gudnason, C. Kouvaris, and F. Sannino, Phys.Rev. **D73**, 115003 (2006), hep-ph/0603014.
[8] S. B. Gudnason, C. Kouvaris, and F. Sannino, Phys.Rev. **D74**, 095008 (2006), hep-ph/0608055.
[9] E. Nardi, F. Sannino, and A. Strumia, JCAP **0901**, 043 (2009), 0811.4153.
[10] D. E. Kaplan, M. A. Luty, and K. M. Zurek, Phys.Rev. **D79**, 115016 (2009), 0901.4117.
[11] J. Shelton and K. M. Zurek, Phys.Rev. **D82**, 123512 (2010), 1008.1997.
[12] T. Appelquist et al. (LSD Collaboration), Phys.Rev.Lett. **104**, 071601 (2010), 0910.2224.
[13] T. Appelquist et al. (LSD Collaboration), Phys.Rev.Lett. **106**, 231601 (2011), 1009.5967.
[14] R. S. Chivukula and T. P. Walker, Nucl. Phys. **B329**, 445 (1990).
[15] J. Bagnasco, M. Dine, and S. D. Thomas, Phys.Lett. **B320**, 99 (1994), hep-ph/9310290.
[16] R. Foadi, M. T. Frandsen, and F. Sannino, Phys.Rev. **D80**, 037702 (2009), 0812.3406.
[17] M. T. Frandsen and F. Sannino, Phys.Rev. **D81**, 097704 (2010), 0911.1570.
[18] T. Banks, J.-F. Fortin, and S. Thomas (2010), 1007.5515.
[19] G. D. Kribs, T. S. Roy, J. Terning, and K. M. Zurek, Phys. Rev. **D81**, 095001 (2010), 0909.2034.
[20] R. Fok and G. D. Kribs, Phys.Rev. **D84**, 035001 (2011), 1106.3101.
[21] T. Appelquist, R. Babich, R. C. Brower, M. I. Buchoff, M. Cheng, et al., Phys.Rev. **D85**, 074505 (2012), 1201.3977.
[22] S. Syritsyn, J. Bratt, M. Lin, H. Meyer, J. Negele, et al., Phys.Rev. **D81**, 034507 (2010), 0907.4194.
[23] J. Green, S. Krieg, J. Negele, A. Pochinsky, and S. Syritsyn, PoS **LATTICE2011**, 157 (2011), 1111.0255.
[24] J. Beringer et al. (Particle Data Group), Phys.Rev. **D86**, 010001 (2012).
[25] S. Collins, M. Gockeler, P. Hagler, R. Horsley, Y. Nakamura, et al., Phys.Rev. **D84**, 074507 (2011), 1106.3580.
[26] J. Green, M. Engelhardt, S. Krieg, J. Negele, A. Pochinsky, et al. (2012), 1209.1687.
[27] M. Lin (RBC/UKQCD Collaborations), PoS **LAT-**

TICE2012, 172 (2013), 1303.0022.
[28] E. Aprile et al. (XENON100 Collaboration) (2012), 1207.5988.
[29] C. Handbook, Lide, D. R., Ed (1986).
[30] J. Lewin and P. Smith, Astropart.Phys. **6**, 87 (1996).
[31] A. L. Fitzpatrick, W. Haxton, E. Katz, N. Lubbers, and Y. Xu (2012), 1203.3542.
[32] A. L. Fitzpatrick, W. Haxton, E. Katz, N. Lubbers, and Y. Xu (2012), 1211.2818.
[33] R. Lewis, C. Pica, and F. Sannino, Phys.Rev. **D85**, 014504 (2012), 1109.3513.
[34] A. Hietanen, C. Pica, F. Sannino, and U. I. Sondergaard (2012), 1211.5021.
[35] A. Belyaev, M. T. Frandsen, S. Sarkar, and F. Sannino, Phys.Rev. **D83**, 015007 (2011), 1007.4839.
[36] Y. Bai and R. J. Hill, Phys.Rev. **D82**, 111701 (2010), 1005.0008.
[37] M. Frigerio, A. Pomarol, F. Riva, and A. Urbano, JHEP **1207**, 015 (2012), 1204.2808.
[38] M. R. Buckley and E. T. Neil (2012), 1209.6054.
[39] Depending on other symmetry considerations, the pseudo-Goldstone bosons could also play the role of dark matter [35–38].
[40] Sign conventions of the isovector and isoscalar form factors are chosen to agree with nuclear physics notations; since we use the neutron (udd) as our in- and out-states, we have to swap $u \longleftrightarrow d$ in the r.h.s of Eq. 2.
[41] We denote the observables associated with the neutral dark baryon in our calculations with the subscript "neut" to avoid confusion with the QCD neutron, for which we reserve the subscript "n".
[42] In comparison to the differential cross-section in Ref. [18], Eq. (22) is the full spin-independent amplitude taking into account the non-trivial electric form factor of a DM particle, $G_{E\chi}(Q^2) = -\frac{1}{6}Q^2 r_{E\chi}^2 + \mathcal{O}(Q^4)$. With the Dirac radius set to zero, $r_{1\chi}^2 = r_{E\chi}^2 - \frac{3\kappa_\chi}{2m_\chi^2} = 0$, Eq. (22) reproduces identically the results in Ref. [18] with $g_M = \frac{1}{2}\kappa_\chi$ and zero electric dipole moment ($g_E = 0$).